The Cryosphere
Discussions

Open Access

The GAMDAM Glacier Inventory: a quality controlled inventory of Asian glaciers

T. Nuimura[1,a], A. Sakai[1], K. Taniguchi[1,b], H. Nagai[1,c], D. Lamsal[1], S. Tsutaki[1,d,e],
A. Kozawa[1], Y. Hoshina[1], S. Takenaka[1], S. Omiya[1,f], K. Tsunematsu[1,g],
P. Tshering[1], and K. Fujita[1]

[1]Graduate School of Environmental Studies, Nagoya University, Nagoya, Japan
[a]now at: Chiba Institute of Science, Chiba, Japan
[b]now at: Center for Research in Isotopes and Environmental Dynamics, University of
Tsukuba, Tsukuba, Japan
[c]now at: Japan Aerospace Exploration Agency, Tsukuba, Japan
[d]now at: National Institute of Polar Research, Tachikawa, Japan
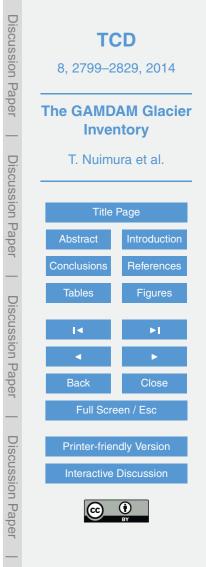[e]now at: Institute of Low Temperature Science, Hokkaido University, Sapporo, Japan
[f]now at: Civil Engineering Research Institute for Cold Region, Sapporo, Japan
[g]now at: Yamanashi Institute of Environmental Sciences, Yamanashi, Japan

Correspondence to: T. Nuimura (tnuimura@cis.ac.jp)

Title Page

Abstract	Introduction
Conclusions	References
Tables	Figures

|◄ | ►|

◄ | ►

Back | Close

Full Screen / Esc

Printer-friendly Version

Interactive Discussion

Abstract

We present a new glacier inventory for the high mountain Asia named "Glacier Area Mapping for Discharge from the Asian Mountains" (GAMDAM). Glacier outlines were delineated manually using more than 226 Landsat ETM+ scenes from the period 1999–2003, in conjunction with a digital elevation model (DEM) and high-resolution Google Earth imagery. Geolocations are consistent between the Landsat imagery and DEM due to systematic radiometric and geometric corrections made by the United States Geological Survey. We performed repeated delineation tests and rigorous peer review of all scenes used in order to maintain the consistency and quality of the inventory. Our GAMDAM Glacier Inventory (GGI) includes 82 776 glaciers covering a total area of 87 507 ± 13 126 km^2 in the high mountain Asia. Thus, our inventory represents a greater number (+4 %) of glaciers but significantly less surface area (−31 %) than a recent global glacier inventory (Randolph Glacier Inventory, RGI). The employed definition of the upper boundaries of glaciers, glacier recession since the 1970s, and misinterpretation of seasonal snow cover are likely causes of discrepancies between the inventories, though it is difficult to evaluate these effects quantitatively. The GGI will help improve the temporal consistency of the RGI, which incorporated glacier outlines from the 1970s for the Tibetan Plateau, and will provide new opportunities to study Asian glaciers.

1 Introduction

The state and fate of Asian glaciers have important implications for both regional water resources (e.g. Immerzeel et al., 2010; Kaser et al., 2010) and future sea level rise (e.g. Radić and Hock, 2011; Gardner et al., 2013). Changes in glacier mass have been documented and/or estimated using a variety of approaches, such as in situ measurements (Fujita and Nuimura, 2011; Yao et al., 2012), numerical modelling (Immerzeel et al., 2010; Radić and Hock, 2011), and remote sensing (Matsuo and Heki, 2010; Ja-
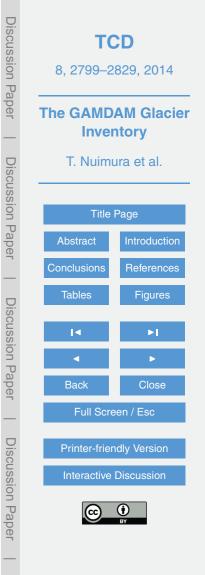
cob et al., 2012; Kääb et al., 2012; Gardner et al., 2013), in order to understand modern spatial variability in the high mountain Asia. However, considerable discrepancies exist among the different studies (e.g. Cogley, 2012; Gardner et al., 2013).

Glacier inventory is a fundamental component in regional projections of mass-balance and glacier discharge. For example, glacier hypsometry (area-elevation distribution) directly affects estimates of mass balance, discharge, and modelled contribution to sea-level rise (Raper et al., 2005), while glacier outline influences projections of mass changes using laser altimetry (Kääb et al., 2012; Gardner et al., 2013). To contribute to the Fifth Assessment of the Intergovernmental Panel on Climate Change (IPCC), the global Randolph Glacier Inventory (RGI) was published (Arendt et al., 2012; Pfeffer et al., 2014). However, while the majority of glacier-outline data used in that study were derived from recent satellite imagery, glacier extents in China were incorporated from an inventory dating to the 1970s (Shi, 2008). Furthermore, a quarter of glacier-area measurements and half of the glacier counts used in the RGI are undated because priority was given instead to global coverage (Pheffer et al., 2014).

We launched a project, entitled Glacier Area Mapping for Discharge in Asian Mountains (GAMDAM), to investigate the contribution of glacier meltwater to Asian river systems since 2011. Here, we describe the materials and procedures used to delineate glacier outlines over the high mountain Asia, and show a preliminary comparison of our GAMDAM Glacier Inventory with the RGI.

Our target region covers the high mountain Asia between 66.5–104.5° E longitude and 26.5–55.5° N latitude, which corresponds to the regions of Central Asia, South Asia West, South Asia East and Altay and Sayan of North Asia in RGI (Arendt et al., 2012; Pfeffer et al., 2014). Pfeffer et al. (2014) have provided $62\,606\,km^2$ with 8.4 % error, $33\,859\,km^2$ with 7.7 % error, $21\,799\,km^2$ with 8.3 % error, and $3430\,km^2$ with 10.3 % error in each region.
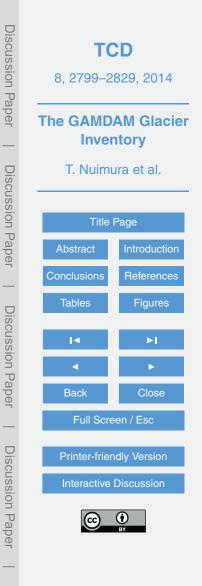
2   Datasets

We analysed 226 Landsat level 1 terrain-corrected (L1T) scenes available from USGS EarthExplorer (http://earthexplorer.usgs.gov/), for the period 1999–2003 (Table S1), prior to the 2003 failure of the scan line corrector (SLC). Systematic radiometric and geometric corrections were performed for the L1T imagery using Global Land Survey 2000, for absolute geodetic accuracy, and the SRTM (http://landsat.usgs.gov/Landsat_Processing_Details.php) digital elevation model (DEM). We selected scenes with minimal cloud and snow cover from paths 130–154 and rows 22–41 in the Worldwide Reference System. In regions where seasonal snow and cloud cover frequently hamper the identification of glacier limits (e.g. Karakoram and Hengduan Shan), we used multiple scenes to increase accuracy (Fig. 1). Images lacking glaciers are shown in Fig. 1 as "zero scene". Where appropriate L1T scenes were unavailable, we utilised Landsat TM scenes from prior to 1999 (two scenes, Table S1).

To delineate glacier outlines topographically, we used contours (20 m intervals) and slope distribution overlain on the satellite scenes. These topographic data were generated using a gap-filled DEM from the Shuttle Radar Topography Mission (SRTM; Jarvis et al., 2008) and are compatible with the L1T imagery because the latter is corrected using the SRTM. However, we note that the ASTER GDEM reportedly exhibits superior accuracy to the SRTM (Hayakawa et al., 2008). Therefore, in our analysis of median glacier elevation, we compared the SRTM and the most recent version of the GDEM (GDEM2, released in 2011) using the laser-altimetry product ICESat GLA14 (Kääb, 2008).
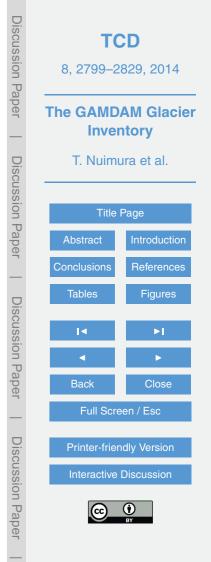
3   Methods

3.1   Pre-processing

We used the Landsat scenes to generate both true-colour (bands 3, 2, 1 as RGB) and false-colour (bands 7, 4, 2 as RGB) composite images at 30 m resolution. True-colour composite images were used primarily for glacier delineation, whereas false-colour images enabled us to differentiate ice from cloud based on the moderately absorptive nature of ice at near-infrared wavelength (Racoviteanu et al., 2008). Additionally, we employed thermal-infrared (band 6) at 60 m resolution to identify ice with a thin debris cover. Due to the time-intensive nature of manually delineating glaciers on high-resolution imagery (Bhambri et al., 2011), we did not adopt a pan-sharpening method using 15 m resolution images (band 8).

We generated contour lines, basin polygons, and slope distribution from SRTM data. Contour lines were used to identify glacier outlines. To avoid misinterpretation of ice divides due to potentially erroneous interpolation of the gap-filled SRTM (Frey et al., 2012), we chose not to use basin polygons to separate ice divides automatically. Instead, basin polygons provided a reference for the manual separation of glacier limits within shared accumulation zones. We paid particular attention to the continuity of glacier ice in areas with steep slopes (> 40°).

3.2   Criteria for manual delineation

In accordance with the Global Land Ice Measurements from Space (GLIMS) protocol (Raup and Khalsa, 2007; Racoviteanu et al., 2009), we defined glacier area as a continuous body of ice. Thus, our measurements do not include steep headwalls located at the upper boundaries of glaciers, where snow does not accumulate but instead is avalanched onto the glacier below (Fig. S1a). Where glacier surfaces are largely free of debris, delineation of the ice surface was possible using true-colour composite imagery (Fig. S1b). On debris-mantled glaciers, false-colour imagery was
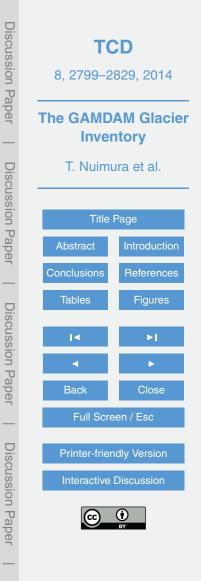
required to identify glacier boundaries (Fig. S1c), while particularly indistinct boundaries in debris-covered ablation zones were delineated by reference to topographic data. Identification of thermokarst features, such as rugged surface topography, was verified using high-resolution Google Earth[TM] images (Fig. S1d). On debris-mantled glacier surfaces, areas of relatively thin debris cover were delineated using thermal infrared band (Fig. S1e). To discriminate between glacier ice and seasonal snow/ice cover, we referred to topographic data (e.g. contour-line spacing). Additionally, Google Earth[TM] imagery and SLC-off scenes (Landsat ETM+ post-dating May 2003) were used to identify ambiguous glacier boundaries, though we note their acquisition dates are different from those of L1T scenes. Some glacier-like areas visible on Landsat scenes were identified later as seasonal snow on images of Google Earth[TM] (Fig. S1f), and vice versa (Fig. S1g).

3.3 Quality control

Considerable variability among measurements of glacier area is possible owing to different interpretations of glacier boundaries (Paul et al., 2013), as well as personnel changes over the course of the project. Figure S2 depicts several examples where glacier boundaries were delineated inaccurately. For example, in the early phase of the project, one operator failed to identify part of an accumulation zone located above an icefall, while a second operator included a steep headwall on which surface features were obscured by shading (Fig. S2a). Similarly, misidentification of glacier boundaries was made in the ablation zone of a debris-covered glacier, where operators erroneously included the lateral moraine (Fig. S2b). Therefore, we conducted a total of five delineation tests in order to ensure adherence to the delineation criteria and to homogenise the quality of our inventory. Accordingly, the errors described above were corrected and the operators were advised of these problems.

Initial delineation of glacier outlines was carried out by 11 operators over a period of 20 months, during which time the quality of delineation might have varied significantly. Therefore, each initial delineation measurement was reviewed and, if necessary, re-

vised by a second operator. Following this peer review of glacier outlines, topological properties were checked. For example, overlapping polygons may cause overestimation of glacier area (Fig. S3a), while irregular polygons (e.g. self-intersecting polygons; Fig. S3b) cannot represent the glacier area accurately. Such misdelineations were detected automatically by GIS functions and then corrected.

3.4 Attribute data

We attached 15 attribute datasets to each glacier analysed. Each glacier is assigned a unique ID consisting of a sequential 6-digit number increasing with the path and row numbers of Landsat (e.g. from p130r037, p130r038 to p154r032, p154r033). Path, row, granule ID, and acquisition date of the Landsat scene, as well as the name of the operator, are included to enable traceability and validation by others. In addition, basic geographic information, such as longitude, latitude, and area, are provided together with elevation data (mean, median, maximum, minimum, range, and mid), which were derived from GDEM2 (Table S2). We also provided records of the peer review and revision of glacier outlines (reviewer name and date) that were performed on each scene (Table S3). These records will permit others to validate our inventory and analyse changes in glacier extent over time using another inventory.

4 Results

4.1 Digital elevation models

As described above, we used the gap-filled SRTM DEM to delineate glacier outlines because of its widespread use and reputation as a high-quality global DEM. Nonetheless, we acknowledge that the accuracy of the recently released ASTER GDEM2 may exceed that of the SRTM (e.g. Hayakawa et al., 2008). Therefore, we tested the SRTM and GDEM2 using glacier polygons in which our data show elevation differences between DEMs of > 100 m. We then compared each DEM with the ICESat GLA 14
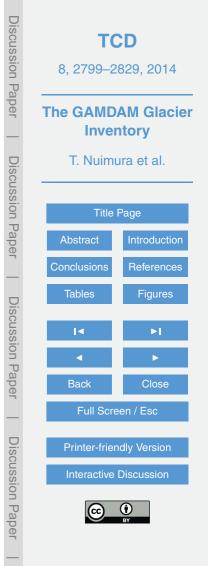
(Fig. 2a). We found that elevations of the GDEM2 are consistent with those of ICESat, showing a slight bias of +40 m, while those of the SRTM show a significantly negative bias (−99 m) and a large analytical uncertainty (Fig. 2b).

The distribution of elevation differences indicates that significant biases in the SRTM occur along the Karakorum and Himalayas, while those of the GDEM2 are focused on the central Tibetan Plateau (Fig. 2c). In the Karakorum and Himalayas, high-relief topography probably resulted in numerous voids in the original SRTM-3 product (Frey et al., 2012), thereby resulting in the considerable biases observed there. Meanwhile, the low relief and less colour contrast of snow field on the Tibetan Plateau may be responsible for the large uncertainty in the GDEM2, which was created by optical stereo photogrammetry (Toutin, 2002). Therefore, we used the GDEM2 for the following median-elevation analyses.

4.2 Evaluation of uncertainties

Uncertainty in glacier delineation was evaluated using the results of five separate delineation tests (Fig. 3). We defined uncertainty as one normalised standard deviation. This was calculated as the standard deviation of the glacier area as measured by different operators, divided by the glacier area included in the final GAMDAM Glacier Inventory (GGI). Figure 3 shows that the normalised standard deviation decreases with increasing glacier area. While linear improvement throughout the delineation test is not evident, the large normalised standard deviations ($> 25\%$) of small glaciers ($< 2.5\,\mathrm{km}^2$), which are evident in tests 1–4, disappear in the final (5th) test. Large glaciers ($> 2.5\,\mathrm{km}^2$) exhibit lower normalised standard deviations ($< 15\%$) than small glaciers. A debris-covered glacier gives a normalised standard deviation of approximately 10 %. In summary, the uncertainty of delineated glacier areas in the GGI is less than 25 % for small glaciers ($< 2.5\,\mathrm{km}^2$) and $\sim 15\%$ for large glaciers ($> 2.5\,\mathrm{km}^2$). Therefore, we expect approximately 15 % uncertainty in our glacial area computation.

The GAMDAM Glacier Inventory

T. Nuimura et al.

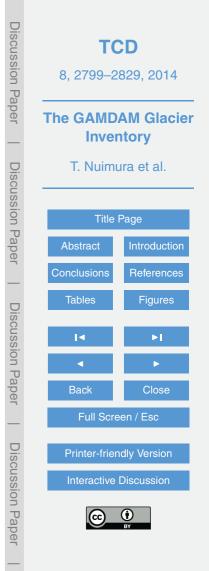## 4.3 Distribution of glaciers and their median elevations

We delineated a total of 82 776 glaciers with a total area of $87\,507 \pm 13\,126\,km^2$ in the high mountain Asia (Table 1). Figure 4 shows the distribution of median glacier elevations based on the GDEM2 and contour lines. Values represent the area-weighted average of median elevations within each 0.5° grid. This figure also shows the distribution of snow-line elevations estimated by Shi (2008). Although it is unclear which data and methods were used to generate this dataset, large-scale features evident in the distribution of snow-line elevations are consistent with our median-glacier elevations. These include a pronounced trough in south-eastern Tibet, caused by intense precipitation along the Brahmaputra River (Liu et al., 2006; He, 2003), and a crest in western Tibet resulting from the prevailing arid, cold climate (Shangguan et al., 2007).

5 Discussion

5.1 Comparison of inventories in the Bhutan Himalaya

We compared our GGI with two other glacier inventories, the RGI version 3.2 (Arendt et al., 2012; Pfeffer et al., 2014) and a glacier inventory derived from high-resolution (2.5 m) Advanced Land Observing Satellite imagery (AGI) from the Bhutan Himalaya. Glacier outlines in the AGI were delineated manually using criteria similar to those of the GGI (Nagai et al., 2013, 2014). In the following analysis, glaciers smaller than $0.05\,km^2$ were excluded from all inventories. The number of glaciers and glacier area are highly consistent between the GGI and AGI (101 % in number and 99 % in area), while those of the RGI are significantly greater than the AGI (115 % in number and 154 % in area). Distributions of number and area data suggest that glaciers greater than $0.5\,km^2$ in area are significantly over-delineated in the RGI relative to those in GGI and AGI, while small glaciers ($< 0.5\,km^2$) are undelineated in the RGI. This pattern may result from the coarse resolution of remotely sensed imagery (Fig. 5). In contrast,
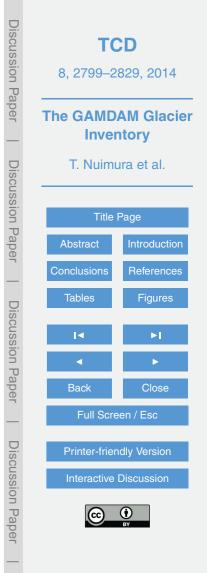
the GGI and AGI show similar number and area distributions regardless of glacier size. Hypsometries of the three inventories also suggest that the RGI over-delineates glaciers at all elevations, relative to the GGI and AGI (Fig. 6a). We note that no glacier is found in either the GGI or AGI below 4000 m elevation.

5   To determine where the RGI over-delineates glaciers, we depicted the spatial distribution of the area-weighted mean of median-glacier elevation in each 0.1° grid for all three inventories (Fig. 7). Our analysis reveals that the RGI depicts glaciers with median elevation lower than 4800 m in south-east Bhutan, where no glacier was identified in either the AGI and GGI. Moreover, upon visual inspection, we found no landforms suggesting the pre-existence of glaciers in this region. Therefore, we suggest that the

10   RGI has misinterpreted seasonal snow cover as glacier ice. We also compared scattergrams of RGI- and GGI-derived glacier number, area, and median-elevation values in the same 0.1° grid to those for the AGI (Fig. 8). Although we found no clear trends in terms of number of glaciers, we note that the RGI delineated glaciers where none were identified in the AGI (points along zero in the x-axis, Fig. 8a). In contrast, Fig. 8b

15   indicates that glacier area was over-delineated in the RGI relative to both the GGI and AGI. Finally, the area-weighted means of median glacier elevation also show a high degree of consistency between the GGI and AGI, whereas lower-elevation glaciers were misinterpreted in RGI (though some grids are not depicted due to no data in the AGI)

20   (Fig. 8c).

5.2   Comparison of inventories in the high mountain Asia

For a more regional-scale test, we compared the GGI and RGI across the high mountain Asia. Whereas the total number of glaciers in the GGI was slightly higher (by 3338, or +4%) than in the RGI, total glacier area was significantly reduced (by 38 554 km^2,

25   or −31%) relative to the RGI, a degree of difference similar to that observed in the Bhutan Himalaya. The significant over-delineation of glacier area by the RGI occurs at all elevations (Fig. 6b). Size distributions of glacier number and area also exhibit relationships similar to those in the Bhutan Himalaya, with the RGI over-delineating

glaciers larger than $0.5\,km^2$ and under-delineating small ($< 0.5\,km^2$) glaciers (Fig. 9). The greater number and area of small glaciers in the GGI may result from our manual glacier partitioning using the basin polygons. In contrast, the RGI incorporates glaciers identified automatically using spectral characteristics, potentially resulting in incomplete partitioning (Fig. 10).

We evaluated spatial distributions of glacier number and area in each 0.5° grid to assess the discrepancy between the inventories (Fig. 11). We found that both number and area are greater in the RGI than in the GGI throughout the Himalayas, whereas significant over-counting of glacier number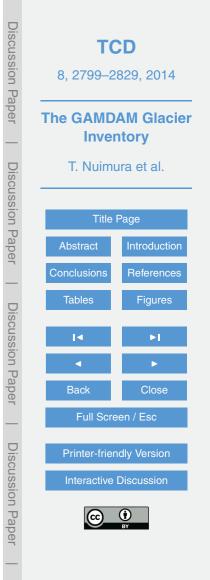s is evident in the GGI for the western Tien Shan, Pamir, Karakorum, and Hengduan Shan. Minor over-counting in the GGI occurs over the Tibetan Plateau (Fig. 11a). Over-delineation of glacier area in the GGI occurs only in the western part of the high mountain Asia, where no glaciers are found in the RGI (Fig. 11b).

We also analysed distributions of area difference in both the upper and lower zones of glaciers, distinguished by the median elevation, in each 0.5° grid. We calculate the normalised difference (D_N, %) as follows:

$$D_N = \frac{v_{RGI} - v_{GGI}}{v_{GGI}} \times 100, \qquad (1)$$

where the variable (v) is the glacier area, or number of glaciers, in each 0.5° grid, and the subscript denotes the inventory. Area-weighted means of median elevation in the GGI were used to distinguish between the upper and lower zones for both inventories (Fig. 12). While we cannot assume that significant shifts in median elevation within both inventories would not result in different glacier hypsometries (Fig. 6), the relatively minor differences observed in the upper zones of Tibetan glaciers potentially result from the limited disparity between delineations in the GGI and RGI (Fig. 12a). This effect is probably due to the relatively low topographic relief on the Tibetan Plateau. Some over-delineation of the upper zone in the RGI occurs around the periphery of the Tibetan Plateau, where high-relief headwalls might have been included as a part of glacier

extent (Fig. 10d). As noted above, such topography was excluded in the GGI and AGI (Nagai et al., 2013, 2014). In contrast, lower zones in the RGI are over-delineated throughout much of the high mountain Asia (Fig. 12b). Although this over-delineation could be the result of real changes in glacier extent on the Tibetan Plateau since the 1970s (Shangguan et al., 2007), we cannot exclude the possibility that the discrepancy reflects misinterpretation of seasonal snow cover at lower elevations (Fig. 10c).
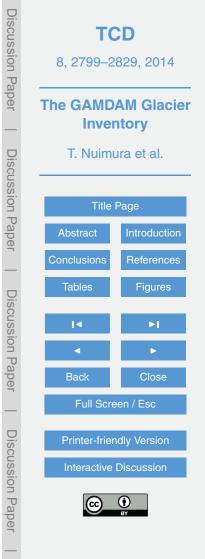
Additionally, we also performed regional comparison of glacier determined by GGI against those of RGI reported by Bajracharya and Shrestha (2011) and Bolch et al. (2012) over Himalaya and Karakoram region. Tables 2 and 3 show summary of total glacier area in each region reported by Bajracharya and Shrestha (2011), Bolch et al. (2012) and GGI. Their source satellite data were Landsat ETM+ imagery taken after 2000. Therefore, the time difference against GGI is relatively smaller. The discrepancy of glacier area of Bajracharya and Shrestha (2011) and Bolch et al. (2012) relative to GGI is 12 % and 22 % respectively, slightly smaller than the difference between GGI and RGI in the entire area (31 %). Therefore, the discrepancy could include both real changes in glacier extent on the Tibetan Plateau since 1970s and misinterpretation of seasonal snow cover at lower elevations (Fig. 10c).

6   Conclusions

We presented a new glacier inventory for the high mountain Asia based primarily on ortho-calibrated Landsat ETM+ scenes from the period 1999–2003. Although both time- and labour-intensive, our manual-delineation approach and rigorous peer-review process (Fig. 3; Table S3) reinforce our confidence in the quality of glacier outlines incorporated in the GGI. Consequently, the GGI will improve the homogenised temporal consistency of the global-scale RGI, which currently incorporates glacier outlines from the 1970s in parts of China (Pfeffer et al., 2014).

Our comparison of the GGI and RGI revealed that glacier numbers in the former are slightly greater (+4 %) than in the latter. Conversely, total glacier area is signifi-

cantly less (−31 %) in the GGI than in the RGI (Table 1). Definition of glacier extent, such as the inclusion or exclusion of upper headwalls, potentially accounts for some of the discrepancy found in the upper zones of glaciers in these high-relief mountain regions (Fig. 12a). Recent glacier recession has probably exacerbated the disparity between inventories, since the source data of the RGI dates to the 1970s. Unfortunately, misinterpretation of seasonal snow cover at lower elevations (Fig. S1c) makes the quantitative evaluation of glacier change problematic.

The large discrepancies in glacier area between the two inventories have important implications for projections of glacier change in this region. For example, the significantly smaller area represented in the GGI will result in drastic changes in glacier area when compared with former snapshots (e.g. the 1970s in the RGI). Conversely, the exclusion of upper headwalls and seasonal snow in the GGI has great potential to correct any discrepancy among projections of mass balances by in situ observations and laser altimetry (Gardner et al., 2013).
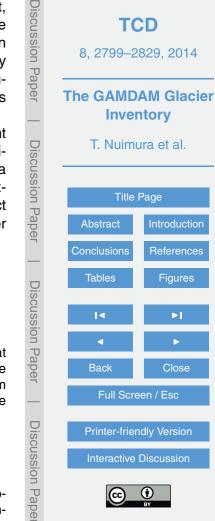
The Supplement related to this article is available online at doi:10.5194/tcd-8-2799-2014-supplement.

References

Arendt, A., Bolch, T., Cogley, J. G., Gardner, A., Hagen, J., Hock, R., Kaser, G., Pfeffer, W., Moholdt, G., Paul, F., Radić, V., Andreassen, L., Bajracharya, S., Beedle, M., Berthier, E., Bhambri, R., Bliss, A., Brown, I., Burgess, E., Burgess, D., Cawkwell, F., Chinn, T., Copland, L.,

Davies, B., de Angelis, H., Dolgova, E., Filbert, K., Forester, R., Fountain, A., Frey, H., Giffen, B., Glasser, N., Gurney, S., Hagg, W., Hall, D., Haritashya, U., Hartmann, G., Helm, C., Herreid, S., Howat, I., Kapustin, G., Khromova, T., Kienholz, C., Köonig, M., Kohler, J., Kriegel, D., Kutuzov, S., Lavrentiev, I., LeBris, R., Lund, J., Manley, W., Mayer, C., Miles, E., Li, X., Menounos, B., Mercer, A., Mölg, N., Mool, P., Nosenko, G., Negrete, A., Nuth, C., Pettersson, R., Racoviteanu, A., Ranzi, R., Rastner, P., Rau, F., Rich, J., Rott, H., Schneider, C., Seliverstov, Y., Sharp, M., Sigurosson, O., Stokes, C., Wheate, R., Winsvold, S., Wolken, G., Wyatt, F., and Zheltyhina, N.: Randolph Glacier Inventory – a Dataset of Global Glacier Outlines: Version 3.2, Global Land Ice Measurements from Space, Boulder Colorad, USA, Digital Media, http://www.glims.org/RGI/randolph.html, 2012.

Bajracharya, S. R. and Shrestha, B. (Eds.): The status of glaciers in the Hindu Kush-Himalayan regtion, International Centre for Integrated Mountain Development, Kathmandu. 2011.

Bhambri, R., Bolch, T., and Chaujar, R.: Mapping of debris-covered glaciers in the Garhwal Himalayas using ASTER DEMs and thermal data, Int. J. Remote Sens., 32, 8095–8119, 2011.

Bolch, T., Kulkarni, A., Kääb, A., Huggel, C., Paul, F., Cogley, J. G., Frey, H., Kargel, J. S., Fujita, K., Scheel, M., Bajracharya, S., and Stoffel, M.: The state and fate of Himalayan Glaciers, Science, 336, 310–314, 2012.
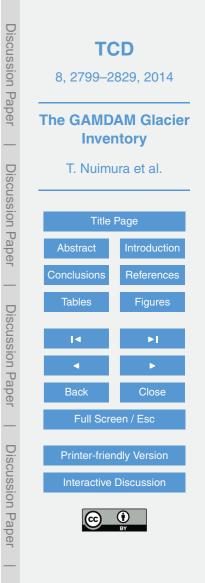
Cogley, J. G.: Climate science: Himalayan glaciers in the balance, Nature, 488, 468–469, doi:10.1038/488468a, 2012.

Frey, H., Paul, F., and Strozzi, T.: Compilation of a glacier inventory for the western Himalayas from satellite data: methods, challenges, and results, Remote Sens. Environ., 124, 832–843, doi:10.1016/j.rse.2012.06.020, 2012.

Fujita, K. and Nuimura, T.: Spatially heterogeneous wastage of Himalayan glaciers, P. Natl. Acad. Sci. USA, 108, 14011–14014, 2011.

Gardner, A., Moholdt, G., Cogley, J., Wouters, B., Arendt, A., Wahr, J., Berthier, E., Hock, R., Pfeffer, W., Kaser, G., Ligtenberg, S., Bolch, T., Sharp, M., Hagen, J., van den Broeke, M., and Paul, F.: A reconciled estimate of glacier contributions to sea level rise: 2003 to 2009, Science, 340, 852–857, doi:10.1126/science.1234532, 2013.

Hayakawa, Y., Oguchi, T., and Lin, Z.: Comparison of new and existing global digital elevation models: ASTER G-DEM and SRTM-3, Geophys. Res. Lett., 35, L17404, doi:10.1029/2008GL035036, 2008.

The GAMDAM Glacier Inventory

T. Nuimura et al.

Title Page

Abstract	Introduction
Conclusions	References
Tables	Figures

Back | Close

Full Screen / Esc

Printer-friendly Version

Interactive Discussion

He, Y.: Changing features of the climate and glaciers in China's monsoonal temperate glacier region, J. Geophys. Res, 108, 1–7, doi:10.1029/2002JD003365, 2003.

Immerzeel, W., van Beek, L. P. H., and Bierkens, M.: Climate change will affect the Asian water towers, Science, 328, 1382–1385, doi:10.1126/science.1183188, 2010.

Jacob, T., Wahr, J., Pfeffer, W., and Swenson, S.: Recent contributions of glaciers and ice caps to sea level rise, Nature, 482, 514–518, 2012.

Jarvis, A., Reuter, H., Nelson, A., and Guevar, E.: Hole-filled SRTM for the globe Version 4, available from the CGIAR-CSI SRTM 90m Database, available at: http://srtm.csi.cgiar.org/ (last access: 28 March 2014), 2008.

Kaser, G., Grosshauser, M., and Marzeion, B.: Contribution potential of glaciers to water availability in different climate regimes, P. Natl. Acad. Sci. USA, 107, 20223–20227, 2010.

Kääb, A.: Glacier volume changes using ASTER satellite stereo and ICESat GLAS laser altimetry. A test study on Edgeøya, Eastern Svalbard, IEEE T. Geosci. Remote, 46, 2823–2830, 2008.

Kääb, A., Berthier, E., Nuth, C., Gardelle, J., and Arnaud, Y.: Contrasting patterns of early twenty-first-century glacier mass change in the Himalayas, Nature, 488, 495–498, doi:10.1038/nature11324, 2012.

Liu, S., Shangguan, D., Ding, Y., Han, H., Xie, C., Zhang, Y., Li, J., Wang, J., and Li, G.: Glacier changes during the past century in the Gangrigabu mountains, southeast Qinghai-Xizang (Tibetan) Plateau, China, Ann. Glaciol., 43, 187–193, doi:10.3189/172756406781812348, 2006.

Matsuo, K. and Heki, K.: Time-variable ice loss in Asian high mountains from satellite gravimetry, Earth Planet. Sc. Lett., 290, 30–36, 2010.

Nagai, H., Fujita, K., Nuimura, T., and Sakai, A.: Southwest-facing slopes control the formation of debris-covered glaciers in the Bhutan Himalaya, The Cryosphere, 7, 1303–1314, doi:10.5194/tc-7-1303-2013, 2013.

Nagai, H., Fujita, K., Sakai, A., Nuimura, T., and Tadono, T.: Climatic and topographic influences on glacier distribution in the Bhutan Himalaya, The Cryosphere Discuss., 8, 1305–1336, doi:10.5194/tcd-8-1305-2014, 2014.

Paul, F., Barrand, N., Baumann, S., Berthier, E., Bolch, T., Casey, K., Frey, H., Joshi, S., Konovalov, V., Le Bris, R., Mölg, N., Nosenko, G., Nuth, C., Pope, A., Racoviteanu, A., Rastner, P., Raup, B., Scharrer, K., Steffen, S., and Winsvold, S.: On the accuracy of glacier outlines de-

rived from remote-sensing data, Ann. Glaciol., 54, 171–182, doi:10.3189/2013AoG63A296, 2013.

Pfeffer, W. T., Arendt, A. A., Bliss, A., Bolch, T., Cogley, J. G., Gardner, A. S., Hagen, J. O., Hock, R., Kaser, G., Kienholz, C., Miles, E. S., Moholdt, G., Mölg, N., Paul, F., Radić, V., Rastner, P., Raup, B. H., Rich, J., Sharp. M. J., and THE RANDOLPH CONSORTIUM: the Randolph Glacier Inventory: a globally complete inventory of glaciers, J. Glaciol., 60, 537–552, 2014.

Racoviteanu, A., Williams, A., and Barry, R.: Optical remote sensing of glacier characteristics: a review with focus on the Himalaya, Sensors, 8, 3355–3383, 2008.

Racoviteanu, A., Paul, F., Raup, B., Khalsa, S., and Armstrong, R.: Challenges and recommendations in mapping of glacier parameters from space: results of the 2008 Global Land Ice Measurements from Space (GLIMS) workshop, Boulder, Colorado, USA, Ann. Glaciol., 50, 53–69, doi:10.3189/172756410790595804, 2009.

Radić, V. and Hock, R.: Regionally differentiated contribution of mountain glaciers and ice caps to future sea-level rise, Nat. Geosci., 4, 91–94, doi:10.1038/ngeo1052, 2011.

Raper, S. C. B. and Braithwaite, R.: The potential for sea level rise: new estimates from glacier and ice cap area and volume distributions, Geophys. Res. Lett., 32, L05502, doi:10.1029/2004GL021981, 2005.

Raup, B. and Khalsa, S.: GLIMS analysis tutorial, Boulder, CO, University of Colorado, National Snow and Ice Data Center, available at: http://www.glims.org/MapsAndDocs/guides.html (last access: 28 January 2014), 2007.

Shangguan, D., Liu, S., Ding, Y., Li, J., Zhang, Y., Ding, L., Wang, X., Xie, C., and Li, G.: Glacier changes in the west Kunlun Shan from 1970 to 2001 derived from Landsat TM/ETM+ and Chinese glacier inventory data, Ann. Glaciol., 46, 204–208, doi:10.3189/172756407782871693, 2007.

Shi, Y. (Ed.): Concise Glacier Inventory of China, Shanghai Popular Science Press, China, 2008.

Toutin, T.: Three-dimensional topographic mapping with ASTER stereo data in rugged topography, IEEE T. Geosci. Remote, 40, 2241–2247, 2002.

Yao, X., Liu, S., Sun, M., Wei, J., and Guo, W.: Volume calculation and analysis of the changes in moraine-dammed lakes in the north Himalaya: a case study of Longbasaba lake, J. Glaciol., 58, 753–760, 2012.

Title Page

Abstract	Introduction
Conclusions	References
Tables	Figures

|◄ | ►|

◄ | ►

Back | Close

Full Screen / Esc

Printer-friendly Version

Interactive Discussion

Table 1. Summary of glaciers in the GGI, AGI and RGI. Glaciers smaller than $0.05\,\text{km}^2$ are excluded.

		GGI	AGI	RGI
Bhutan Himalaya	Number of glaciers	1301	1291	1479
	Total Area [km^2]	1488 ± 223	1506	2319
	Number of excluded small glaciers	103	195	83
High mountain Asia	Number of glaciers	82 776	–	79 438
	Total Area [km^2]	87 507±13 126	–	126 051
	Number of excluded small glaciers	7893	–	6137

Table 2. Summary of glaciers in the Bajracharya and Shrestha (2011) and GGI.

Area [km^2]	Bajracharya and Shrestha (2011)	GGI	Difference [km^2]	Difference [%]
Amu Darya	2566	2478	88	104
Indus	21 193	22 125	−932	96
Ganges	9012	5999	3014	150
Brahmaputra	14 020	9417	4603	149
Irrawaddy	35	64	−29	55
Salween	1352	1321	31	102
Mekong	235	225	10	104
Yangtze	1660	1563	97	106
Yellow	137	98	39	139
Tarim Interior	2310	2636	−326	88
Qinghai-Tibetan Interior	7535	7665	−130	98
Total	60 054	53 591	6463	112

Title Page

Abstract | Introduction

Conclusions | References

Tables | Figures

◄ | ►

Back | Close

Full Screen / Esc

Printer-friendly Version

Interactive Discussion

Table 3. Summary of glaciers in the Bolch et al. (2012) and GGI.

Area [km^2]	Bolch et al. (2012)	GGI	Difference [km^2]	Difference [%]
Karakoram	17 946	16 718	1228	107
Western Himalaya	8943	7547	1396	118
Central Himalaya	9940	6491	3449	153
Eastern Himalaya	3946	2701	1245	146
Total	40 775	33 458	7317	122

Full Screen / Esc

Printer-friendly Version

Interactive Discussion

Figure 1. Landsat scenes used in this study to delineate glaciers over high mountain Asia. Zero (black squares) indicates that no glaciers exist in that scene.

Figure 2. Evaluation of DEMs based on ICESat GLA14. Elevations of SRTM and ASTER GDEM version 2 are compared with ICESat GLA14 elevations where large elevation differences (> 100 m) exist between the SRTM and GDEM. **(a)** Scattergram, **(b)** histogram and **(c)** spatial distribution.

Figure 3. Normalised standard deviation of glacier area, based on delineations by different operators and the glacier area used in the final GGI product.

Title Page

Abstract | Introduction

Conclusions | References

Tables | Figures

|◄ | ►|

◄ | ►

Back | Close

Full Screen / Esc

Printer-friendly Version

Interactive Discussion

Figure 4. Distribution of glaciers in the GGI coloured by median elevation. Black contours depict the median elevation of the GGI. Purple contours indicate snow line elevations used in a Chinese glacier inventory (Shi, 2008).
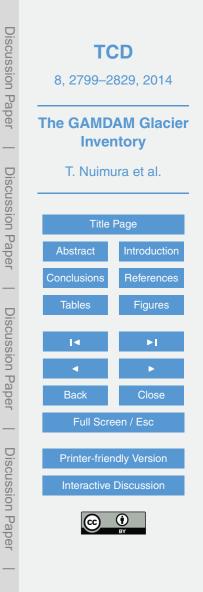
Figure 5. Size distributions of **(a)** number of glaciers and **(b)** glacier area in the Bhutan Himalaya from the GGI, AGI and RGI.

Figure 6. Glacier hypsometries for **(a)** the Bhutan Himalaya and **(b)** the high mountain Asia derived from the GGI, AGI and RGI. Glaciers less than 1 km^2 in area are not included.
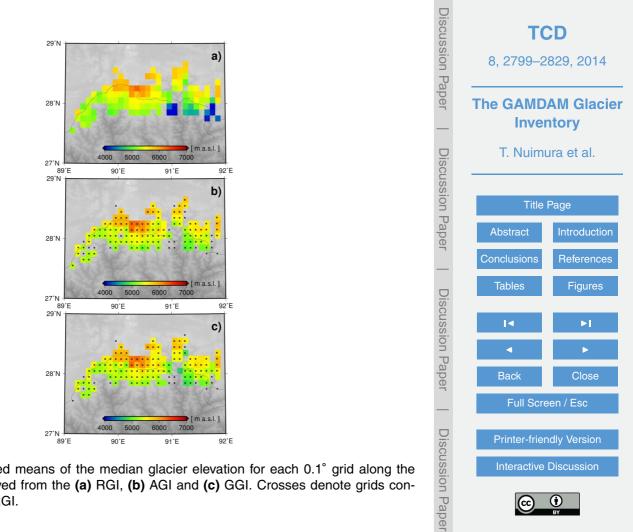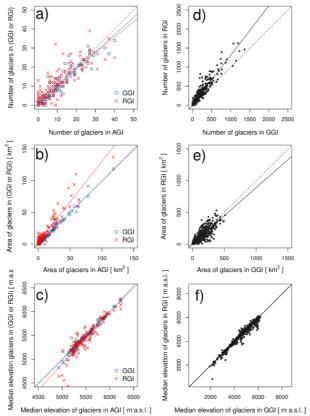
Figure 7. Area-weighted means of the median glacier elevation for each 0.1° grid along the Bhutan Himalaya, derived from the **(a)** RGI, **(b)** AGI and **(c)** GGI. Crosses denote grids containing glaciers in the RGI.

Figure 8. Scattergrams of **(a)** number of glaciers, **(b)** glacier area and **(c)** area-weighted mean of median glacier elevation in each 0.1° grid of the RGI and GGI plotted against the AGI in the Bhutan Himalaya. Scattergrams of **(d)** number of glaciers, **(e)** glacier area and **(f)** area-weighted mean of median glacier elevation in each 0.5° grid of the RGI plotted against the GGI in the high mountain Asia.
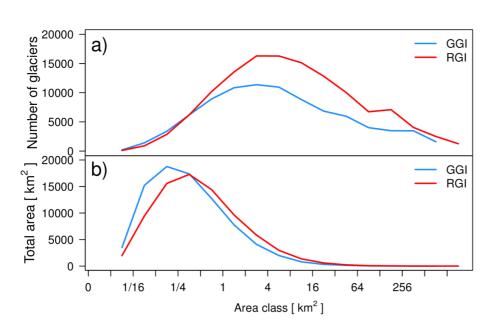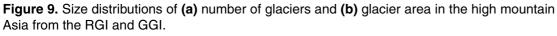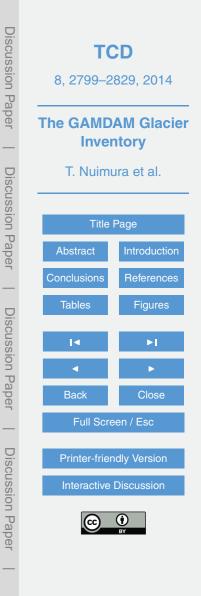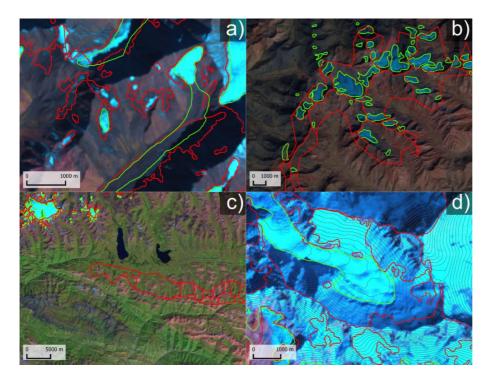
Figure 9. Size distributions of **(a)** number of glaciers and **(b)** glacier area in the high mountain Asia from the RGI and GGI.

Figure 10. Examples of **(a)** seasonally snow-covered areas (76.83° E, 32.50° N), **(b, c)** erroneous polygons (71.28° E, 37.48° N and 95.5° E, 31.5° N), and **(d)** definition differences in upper boundaries in the RGI (red) and GGI (green) (86.88° E, 27.98° N). Grey lines in **(d)** denote contour lines. Background images are true-colour composites of Landsat ETM+ scenes.

Figure 11. Differences between **(a)** number of glaciers and **(b)** glacier area in the RGI and GGI (i.e., RGI – GGI) for each 0.5° grid in the high mountain Asia.

Figure 12. Normalised differences between glacier area in the **(a)** upper and **(b)** lower zones in the RGI and GGI for each 0.5° grid in the high mountain Asia.